JGR Oceans

RESEARCH ARTICLE

Key Points:

- Dynamics of climate-relevant trace gases; N_2O and CH_4 in the Eastern-South Atlantic (ESA)
- Pronounced effect of local sources for CH_4 than N_2O in the Walvis Bay area
- Cape Frio as the greatest source of N_2O and CH_4 to the atmosphere relative to Lüderitz

Supporting Information:

Supporting Information may be found in the online version of this article.

Correspondence to:

B. Sabbaghzadeh,
bita.sabbaghzadeh@io-warnemuende.de

Citation:

Author Contributions:

Methodology: M. Glockzin, S. Otto
Resources: M. Glockzin
Supervision: D. L. Arévalo-Martínez, G. Rehder
Visualization: D. L. Arévalo-Martínez
Writing – review & editing: D. L. Arévalo-Martínez, G. Rehder

Meridional and Cross-Shelf Variability of N_2O and CH_4 in the Eastern-South Atlantic

B. Sabbaghzadeh[1] , **D. L. Arévalo-Martínez[2]** , **M. Glockzin[1]**, **S. Otto[1]**, and **G. Rehder[1]**

[1]Leibniz Institute for Baltic Sea Research, Warnemünde, Germany, [2]GEOMAR Helmholtz Centre for Ocean Research, Kiel, Germany

Abstract Upward transport and/or mixing of trace gas-enriched subsurface waters fosters the exchange of nitrous oxide (N_2O) and methane (CH_4) with the atmosphere in the Eastern-South Atlantic (ESA). To date, it is, however, unclear whether this source is maintained by local production or advection of trace gas-enriched water masses. The meridional and zonal variability of N_2O and CH_4 in the ESA were investigated to identify the contributions of the major regional water masses to the overall budget of N_2O and CH_4. The maximal sea surface N_2O and CH_4 concentrations and the main ESA upwelling cells co-occurred with a strong negative correlation with the sea surface temperature (SST) ($p < 0.05$). The dominance of the central water masses in the winter and spring seasons and the interplay between shelf topography and wind regime are suggested to determine enhanced gas transfer toward the sea-air interface or "capping" at midwater depth. These parameters are supposed to be critical in the local budget of N_2O and CH_4 in the ESA. Our findings also show that the shape of N_2O and CH_4 gradients is very similar both meridionally and zonally; however, the extent of the differences between the high-end and low-end members of the concentrations/saturations range is different. This suggests a more pronounced effect of local sources on CH_4 than N_2O distribution, in particular in the Walvis Bay area. With respect to N_2O, however, low-oxygen waters from the poleward undercurrent impinge in the shelf close to Cape Frio and often result in N_2O concentrations significantly higher than off Lüderitz ($p < 0.05$).

Plain Language Summary The Eastern-South Atlantic (ESA) with some well-documented local upwelling cells is one of the most productive upwelling regions which create hotspots for climate active trace gas production including nitrous oxide (N_2O) and methane (CH_4). N_2O is mainly produced via microbially driven nitrification and denitrification in less oxygenated waters, whereas CH_4 is primarily produced by microbial anaerobic respiration in sediments, and both trace gases are exchanged with the atmosphere in air-sea interface. To what extent the gas distribution and its exchange with the atmosphere is related to water mass advection or local production is still uncertain. Here, we aim to address the contribution of dominant regional water masses to regional trace gas distribution and its atmospheric exchange. We suggest that while there is a more pronounced effect of local sources on CH_4 than N_2O distribution, in particular in the Walvis Bay area, N_2O distribution is more governed by low-oxygen waters from the poleward undercurrent impinging on the shelf close to Cape Frio, deriving significantly higher N_2O concentrations than off Lüderitz ($p < 0.05$).

1. Introduction

Nitrous oxide (N_2O) and methane (CH_4) are long-lived atmospheric trace gases which account for a large fraction of the total radiative forcing due to well-mixed greenhouse gases (GHGs; Myhre, 2013). Albeit a smaller source of atmospheric N_2O and CH_4 in comparison with terrestrial ecosystems, marine environments represent a significant and therefore nonnegligible contribution to their overall budget (Ciais et al., 2013). Overall, the trace gas distribution in the ocean is spatially and vertically heterogeneous due to biogeochemical (microbial) and physical (mixing, upwelling, and stratification) processes, acting either as a trace gas source or sink with respect to the atmosphere (Bates et al., 1996; Reeburgh, 2007).

N_2O is produced in intermediate waters via microbially driven nitrification and denitrification under oxic and suboxic conditions, respectively, and exchanged with the atmosphere in surface waters (Bakker et al., 2014). In the nitrification pathway, carried out by ammonia-oxidizing bacteria and archaea, N_2O is produced as a by-product during the oxidation of NH_4^+ to NO_2^- (Löscher et al., 2012; Ritchie & Nicholas, 1972; Santoro

et al., 2011). Conversely, during bacterial and archeal denitrification, N_2O is an obligate intermediate in the stepwise reduction of NO_3^- to N_2, such that this pathway may represent a source or a sink for this gas, with the enzymes involved on each step being differently affected by environmental conditions, e.g., oxygen concentrations (Zumft, 1997). Alternatively, during nitrifier-denitrification, N_2O can be produced by direct reduction of NO_2^- (Cantera & Stein, 2007).

Oceanic CH_4, on the other hand, is primarily produced by microbial anaerobic respiration with pathways using either CO_2 or acetic acid as electron acceptors instead of oxygen (Bakker et al., 2014). Hence, the largest sources of CH_4 to the water column are anoxic sediments (Middelburg et al., 1996) in oxygen minimum zones (OMZ; Naqvi et al., 2010). CH_4 production via sedimentary methanogenesis is promoted in coastal upwelling regions. Eutrophication and intensification of coastal upwelling due to global warming may also favor methanogenesis (Bakun, 2017; Bakun et al., 2010).

In-situ observations also show that CH_4 may be produced in the anoxic digestive tract of zooplankton and then egested to the oxic water column (Schmale et al., 2018). Alternatively, CH_4 can be released to the water column from sinking organic matter that harbors methanogenic bacteria (Sasakawa et al., 2008), or by in-situ methanogenesis in the surface mixed layer through a variety of different mechanisms, which has been identified as a potential source of atmospheric CH_4 (Klintzsch et al., 2019; Weber et al., 2019). These additional sources can be particularly relevant in shelf areas given the high CH_4 production rates and fast ventilation of the upper water column (Schmale et al., 2018; Stawiarski et al., 2019). The major sinks of CH_4 are aerobic oxidation in the water column and sedimentary anaerobic oxidation associated with sulfate-reducing bacteria (e.g., Boetius et al., 2000; Knittel & Boetius, 2009).

Marine emissions of N_2O and CH_4 to the atmosphere are primarily driven by the gradient in sea-air gas concentration, and also bubble-mediated transfer (ebullition) in the case of CH_4 (Reeburgh, 2007). Such processes are affected by different processes from basin to submesoscale, which might cause interannual variability (see e.g., Arévalo-Martínez et al., 2019; Morgan et al., 2019). In upwelling regions, high surface productivity and nutrient remineralization stimulated by nutrient-rich upwelled waters result in significant fluxes of organic carbon to subsurface waters (Capone & Hutchins, 2013), which, in turn, promotes microbial oxygen consumption and thereby favors the production of N_2O and CH_4 at relatively shallow depths (Frame et al., 2014; Monteiro et al., 2006). Also, high biomass accumulation and the presence of an oxygen minimum zone (OMZ) control biogeochemical processes involved in the cycles of N_2O and CH_4 in upwelling regions (Charpentier et al., 2010; Naqvi et al., 2010). Moreover, intensive vertical advection and mixing drives trace gas-rich underlying waters to the sea surface, enhancing trace gas fluxes to the atmosphere (Charpentier et al., 2010; Frame et al., 2014; Lueker et al., 2003; Nevison et al., 1995).

The Eastern-South Atlantic (ESA) comprises a coastal area characterized by distinctive coastal upwelling systems and a perennial OMZ. It includes the Angola Tropical Zone (ATZ; 6°–14°S), as well as the Benguela upwelling system (BUS; 16°–35°S), which is one of the four major eastern boundary upwelling ecosystems. In this study, we will focus on the ATZ and the northern part of the BUS (nBUS; 16°–27°S). The ATZ is characterized by a clear seasonal cycle with strong stratification in December-March (warm season) and pronounced cooling associated with the uplift of nutrient-enriched deep waters to the surface in July-September (cold season) which is concurrent with the propagation of coastally trapped waves (Hutchings et al., 2009; Tchipalanga et al., 2018). Across the nBUS wind-driven coastal upwelling appears year-round, with discernible intense local upwelling cells such as Cape Frio (18°S), Walvis Bay (23°S) and Lüderitz (26°S). Organic-rich sediment associated with the shallow water depth, makes Walvis Bay one of the hotspots for CH_4 production in the Benguela upwelling region (van der Plas et al., 2007).

Although it is known that the ESA is an overall source of N_2O and CH_4 to the atmosphere due to the occurrence of coastal upwelling, the trace gas fluxes from this region are still poorly quantified (Gutknecht et al., 2013; Naqvi et al., 2010; Nevison et al., 1995, 2004). Earlier studies also suggest that potentially higher emissions from this area are enhanced by lateral advection of gas-rich waters (Gutknecht et al., 2013).

The two major well-documented water masses in the ESA region are the tropical South Atlantic Central Water (SACW) and the subtropical Eastern-South Atlantic Central Water (ESACW), with the transition zone at about 25°S. Nutrient-enriched and oxygen-depleted SACW are transported within the subtropical gyre and the equatorial undercurrent into the Angola-gyre and then advected poleward into the northern Benguela
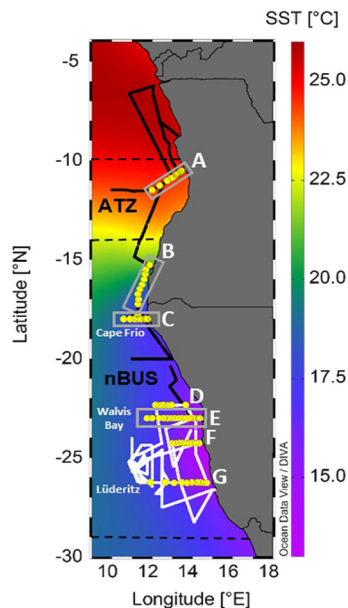
Figure 1. The ship tracks during winter survey (M99, WS; white line) and spring survey (M120, SS; black line). The black dashed lines enclose the spatial domains; Angola Tropical Zone (ATZ) and northern Benguela upwelling system (nBUS). The main upwelling cells include Cape Frio, Walvis Bay, and Lüderitz. The yellow dots represent CTD stations in WS and SS; stations from SS are enclosed by a gray rectangle. Color shading indicates the long-term mean sea surface temperature (SST); data from the World Ocean Atlas (Boyer et al., 2013).

via the Angola Current (Mohrholz et al., 2008; Siegfried et al., 2019). Subtropical ESACW on the other hand is formed in the Cape Basin as a combination of SACW from the subtropical gyre and Indian Central Water (ICW) and is transported northwards by the Benguela Current along the southwest African shelf edge. The movement of these water masses either southward from Cape Frio or northward from Lüderitz, as well as coastal topography and shelf width, may regulate the regional oxygen concentration (Monteiro et al., 2006, 2008). Other local upwelling cells, including Cunene cell (17°S) and northern Namibia (19°S), along with other mesoscale features such as eddies and filaments, result in a dynamic environment with high temporal and spatial variability of N_2O and CH_4 (e.g., Morgan et al., 2019). To date, the few campaigns investigating the biogeochemical properties of the water masses in the region with respect to trace gas cycling suggest a strong influence of aged, low-oxygen, nutrient-rich SACW on the distribution of N_2O and CH_4 (Frame et al., 2014; Monteiro et al., 2006).

In this study, water column and high-resolution continuous surface measurements of N_2O and CH_4 are reported across the ESA, a region with marked zonal gradients, ranging from highly productive coastal upwelling systems in the ESACW to the nutrient-enriched-less oxygenated SACW. The continuous surface measurements reveal characteristics of the trace gas distribution which would not have been detected by discrete sampling. The vertical sections allow for a better understanding of the underlying patterns of these trace gases in the ESA.

We also present a comprehensive analysis of the regional gradients of N_2O and CH_4 emissions to the atmosphere in the ESA region. In particular, we aim to assess the relative contribution of the major water masses to the budget of these trace gases in the water column to better understand the relationship between the production/distribution at midwater depths and the regional trace gas sea-air fluxes.

2. Materials and Methods

2.1. Study Area

The fieldwork took place during the cruises M99 (July 31–August 23, 2013; winter setting (WS)) and M120 (October 17–November 18, 2015; spring setting (SS)) onboard the R/V METEOR, which encompassed close-coastal and open ocean regions off Angola and Namibia. To investigate the regional concentration gradients of N_2O and CH_4 and corresponding sea-air fluxes, seven hydrographic sections (six zonal transects and one alongshore transect) were conducted between ~10° and 26°S (Figure 1).

2.2. Surface (Underway) Measurements of N_2O and CH_4

Concentrations of dissolved N_2O and CH_4 in surface waters were continuously measured by using the Mobile Equilibrator Sensor System (MESS; Figure 2), built at the Trace Gas Biogeochemistry Group of the Leibniz Institute for Baltic Sea Research. For further background and calculations, we refer to Gülzow et al. (2011) and Arévalo-Martínez et al. (2013).

The MESS system comprises a control unit and a custom-built equilibrator which is a combination of bubble-type (e.g., Körtzinger et al., 1996; Schneider et al., 1992) and shower head-type equilibrators (e.g., Johnson, 1999; Figure 2). The equilibrated air is pumped in a closed loop to the cavities of three Cavity Enhanced Absorption Spectrometers (CEAS) in a parallel set up, passing a cool trap, two water guards, and the gas diffuser. In parallel, an external diaphragm pump (KNF Neuberger, Inc.) transports the air in another cycle through the main equilibrator to increase the transfer rate between water and the gaseous phase. To avoid
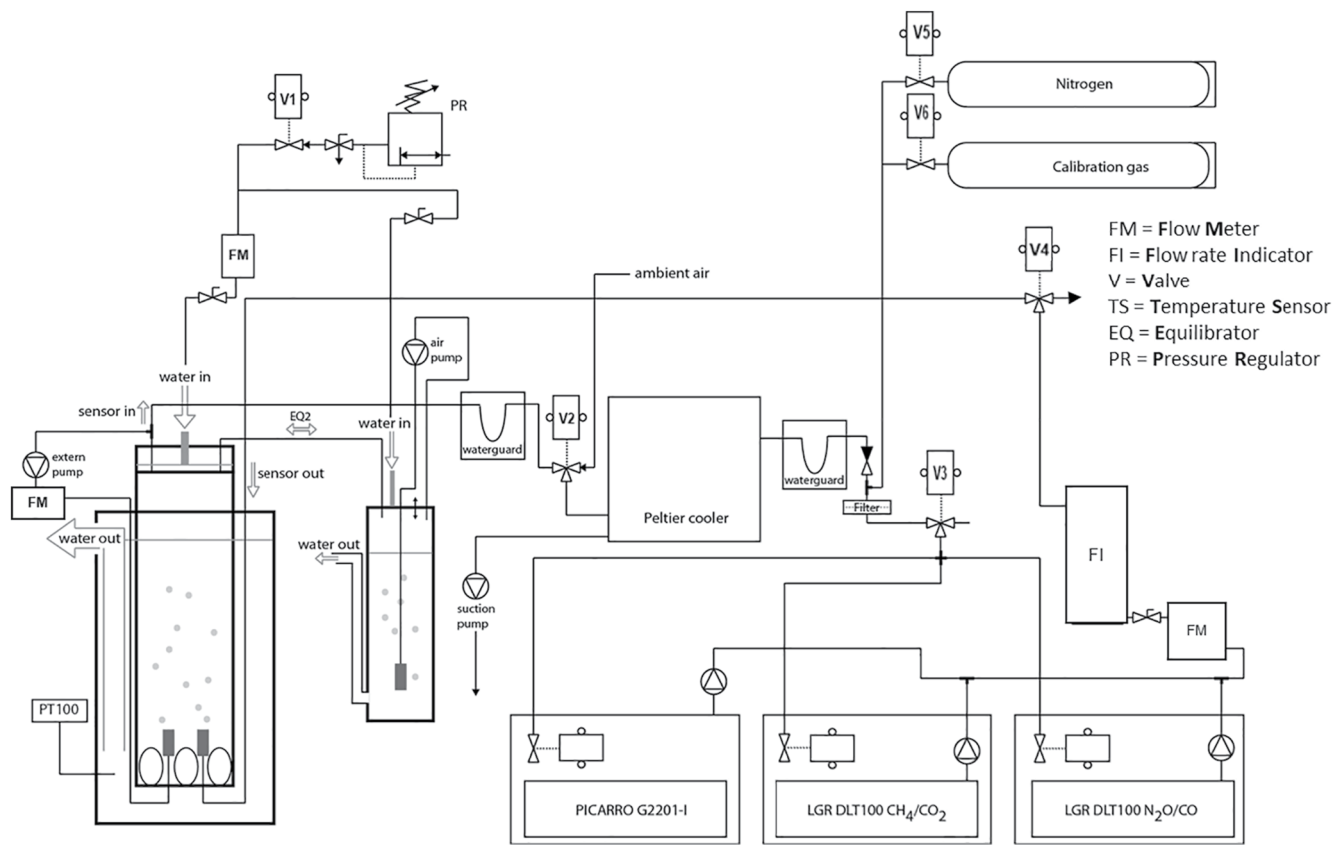
Figure 2. Schematic of the Mobile Equilibrator Sensor System (MESS) used in this study.

an outpouring of gas bubbles caused by the high pressure of the water flow from the shower head, the drain holes at the bottom of the main equilibrator are covered with gauze. This setup was coupled in line with two Los Gatos Research off-axis laser absorption spectroscopy (oa-ICOS) analyzers (CH_4, CO_2, N_2O, CO), and one PICARRO G2131-i cavity ring-down spectrometry (CRDS) analyzer (isotopic CO_2 measurements, not discussed in this manuscript). Tubing is a 6×4 mm polyethylene-coated aluminum foil (Synflex 1,300) connected to stainless steel fittings (Swagelok®).

In this study, for CH_4/CO_2 detection, a DLT 100 Benchtop Model # 908-0011-0001, Los Gatos Research and an RMT 200 Rackmount Model # 907-0010-0001, Los Gatos Research was used on WS (M99) and SS (M120), respectively. For the detection of N_2O/CO, a Benchtop Model # 908-0014-0000, Los Gatos Research was used on both surveys. The principles of laser-based sensors have been described in detail elsewhere (e.g., Baer et al., 2002; Friedrichs et al., 2010; Romanini et al., 1997). More information on surface seawater application can be found in Gülzow et al. (2011) and Arévalo-Martínez et al. (2013).

Seawater was supplied by a deep-well pump (CAPRARI DESERT EX, Italy), installed in the vessel's moonpool at a water depth of ~5.6 m. The flow rate of seawater into the MESS system was maintained between ~8.00 and 9.00 L min^{-1}, and the flow rate of air in the air pump was adjusted between ~4.00 and 5.00 L min^{-1}. The temperature in the equilibrator was determined with a calibrated DOSTMANN P650

equipped with Pt100 temperature probe (accuracy $\pm$ 0.03°C, resolution 0.01°C in the relevant temperature range). All gas analyzers were calibrated using a standard gas at the beginning of the cruise. This gas standard was measured as target daily throughout both surveys for data recalibration and drift correction (Table 1). The results of target measurements were utilized in a two-point linear regression function (forced through zero) that was applied to the sensor data measured until the next target measurement interval. The mean sensor drift was ~0.19 ppb for N_2O and

Table 1
Standard Gas Composition During Winter Setting (WS; M99) and Spring Setting (SS; M120)

Expeditions	Practical gas	N_2O (ppb)	CH_4 (ppb)
WS (M99)	One calibration and target gas	327.85	1900.57
SS (M120)	One calibration and target gas	328.64	1914.60

~0.06 ppb for CH_4 on WS and ~0.12 ppb for N_2O and ~0.04 ppb for CH_4 on SS, estimated from the calibration gas measurements. Additionally, one "zero" gas (Nitrogen 5.0, LINDE) was measured infrequently throughout both cruises for system checks (e.g., leakage detection).

The atmospheric N_2O and CH_4 in ambient air were measured at several sporadic locations, with an inlet installed at 35-m height. The data were quality controlled by comparing with the data generated by NOAA in the nearest atmospheric sampling station (23.58°S, 15.03°E, Station NMB [Gobabeb, Namibia]). The mean dry value of atmospheric N_2O and CH_4 was 325.31 ± 2.44 and 1787.17 ± 2.44 ppb, $n = 21$, respectively, on the WS and 328.44 ± 1.43 and 1798.43 ± 6.74 ppb, $n = 19$, respectively, on the SS, comparable with the mean of 326.06 ± 0.41 ppb, $n = 17$ of atmospheric N_2O and 1786.44 ± 8.00 ppb, $n = 17$ of CH_4 provided by NOAA over the course of the WS. There is no atmospheric N_2O and CH_4 data available from Station NMB during the SS expedition.

2.2.1. Data Processing

Concentrations of N_2O and CH_4 were computed after Arévalo-Martínez et al. (2013) and Gülzow et al. (2011) with solubility coefficients taken from Weiss and Price (1980) and Wiesenburg and Guinasso (1979), respectively. The gas saturations (in %) were subsequently calculated from the concentration ratio between seawater and seawater equilibrated with the atmosphere

$$\text{Saturation} = \left(\frac{C_{\text{sw}}}{C_{\text{eq.sw}}}.100 \right) \tag{1}$$

where C_{sw} is the gas concentration in seawater (nmol L^{-1}) and $C_{\text{eq.sw}}$ is the gas concentration in seawater in equilibrium with the mean atmospheric concentrations measured during the two cruises (see above).

The air-sea gas flux densities (in μmol m^{-2} d^{-1}) were computed as the product of the gas concentration difference between seawater and the sea surface equilibrated with the atmosphere, multiplied by the gas transfer velocity

$$F_{(\text{gas})} = \Delta_{(\text{gas})}.k_w \tag{2}$$

where $F_{(\text{gas})}$ is the flux density of the gas, $\Delta_{(\text{gas})}$ equals $C_{\text{sw}} - C_{\text{eq.atm}}$ for the corresponding gas, and k_w is the gas transfer velocity (Wanninkhof, 2014). The instantaneous wind speeds from the ship's meteorological data were standardized to 10-m height above sea level (U_{10n}) (Large & Pond, 1982). The k_w was then derived from implementing the empirical relationship, $K_{660} = 0.24. U_{10n}^2$ (cm h^{-1}) (Wanninkhof et al., 2009) and the Schmidt number (S_C)

$$k_w = K_{660}.\left(\frac{S_C}{660} \right)^{(-0.5)} \tag{3}$$

The derived data from the analyzers and the auxiliary DSHIP data were uniformly data reduced to one-minute mean values and used for further analysis.

2.3. Water Column (Discrete) Measurements of N_2O and CH_4

Discrete measurements for N_2O on WS were carried out using the dynamic headspace method described in Arévalo-Martínez et al. (2017).

In brief, triplicate bubble-free samples were collected from the 10 L Niskin bottles of a CTD/Rosette (SBE-911 plus SBE 43 O_2 sensor) into 20 mL glass vials at selected locations (Figure 1). To avoid any gas exchange, caution was taken by overfilling the bottles and sealing with a rubber butyl septum and aluminum crimp immediately after sampling. To preserve the samples, 50 μL of saturated $HgCl_2$ solution were added to each bottle. The samples were then stored in dark at 4°C for later analyses within a year. Prior to analysis in the shore-based laboratory, a headspace was created by injection of 10 mL of nitrogen (Linde-Gas, Pullach, Germany) and allowing the excess water to be expelled through a 20 ml plastic syringe. Prior to the measurement, the samples were shaken vigorously for 20 s by using a Vortex-Genie mixer and left upside down

for a minimum of 2 hr, allowing the created headspace to equilibrate with the water. A subsample of the headspace was then drawn and injected into a gas chromatograph (GC; Shimadzu 14B) equipped with an Electron Capture Detector (ECD) for N_2O detection.

The determination of dissolved concentrations of N_2O and CH_4 on SS were carried out using a purge and trap system. The analytical system includes a trap (stainless steel, 700 mm × 1/8", U-shaped) filled with HayeSep D (60/80 mesh, CS Chromatographie Service GmbH, Langerwehe, Germany) to enrich the relevant gas compounds, an injection unit, a purge chamber (200 × 24 mm) with integrated frit (porosity 2, Erich Eydam KG, Kiel, Germany) to purge 20 mL seawater with helium to displace dissolved gases and the GC (Shimadzu GC-2014) to separate gases with a special column circuit to operate in an Electron Capture Detector (ECD) mode for N_2O and a Flame Ionization Detector (FID) mode for CH_4 detection. The technical details were described elsewhere (Wilson et al., 2018). Total runtime (purge and detection time) is 25 min. per sample, with CH_4 detected within the initial 4.5 min. (FID-mode at 200°C) and N_2O detected after 5.5 min. (ECD-mode at 345°C). The system precision for both gases was better than 1%. Two reference gases (i.e., standard gas mixtures with 1533.00 ppb N_2O and 18470.00 ppb CH_4, and 332.00 ppb N_2O and 1880.00 ppb CH_4 with an accuracy better than ±0.2%, in synthetic air; Linde-Gas, Pullach, Germany, recalibrated in house) were measured daily before and after distinct water samples to assess drift behavior on both WS and SS. To determine the standard deviation, the reference gases were measured fourfold and the deviation was lower than 2% and 0.5% for, respectively, N_2O and CH_4.

Prior to the establishment of the purge and trap system, a comparative study with the formerly used headspace method revealed a deviation of <5% between the methods; however, with superior precision and detection limit of the new purge and trap system.

2.3.1. Data Evaluation

As the volume in the calibration loop depends on the temperature (T, in °C) and air pressure (p, mbar), the standard peak area (Area) was corrected, implying the following equation:

$$\text{Area}_{\text{corr}} = \text{Area} \frac{(T + 273.15\text{k})}{(1 / 1013.25 \, \text{mbar}.p)} 273.15 \, \text{k} \tag{4}$$

While CH_4 followed a linear function (i.e., $y = mx + c$), N_2O displayed a quadratic behavior (i.e., $y = ax^2 + bx + c$) and the slope of the function was calculated from the mean of the peak areas. The drift in the sensitivity (m_D) of the system for each individual sample was also calculated as follows:

$$m_{D(N)} = m_{N-1} + \frac{(m_E - m_B)}{(N-1)} \tag{5}$$

where m_E and m_B represent the changes in the sensitivity of the system, determined at the beginning and end of each day's evaluation, and N is the run number of the samples measured on that particular day, respectively. The observed drift over the entire day is usually below 1%.

The CH_4 concentration (nmol L^{-1}) was subsequently calculated, applying the following equation:

$$C_{\text{CH}_4} = \left(\frac{\text{Area}_{\text{sample}}}{m_{D;N}} \right) \cdot \left(\frac{V_{\text{cal. loop}}}{V_{\text{mol}} V_{\text{water}}} \right) 1000 \tag{6}$$

where V_{mol} is the molar gas volume of 22.4 (L mol^{-1}), V_{water} (ml) is the volume of the water sample in the purge vessel, $V_{\text{cal. loop}}$ is the volume of the calibration loop that is, 2.0379 (mL) and Area$_{\text{sample}}$ shows the peak area of the purged sample.

To complete the formula, the relationship between standards (x_{CH_4}; the amount of CH_4 in ppm), the volume of the extracted CH_4 out of the water sample (V_{CH_4} in L), the peak area of the sample (Area$_{\text{sample}}$) and of the standard (Area$_{\text{Std}}$) were also considered in the final two-step equation

$$V_{CH_4} = X_{CH_4} . V_{cal.loop} = \frac{\left(Area_{sample} . X_{CH_4} \right)}{Area_{Std.} V_{Cal.loop}} \tag{7}$$

$$C_{CH_4} = \frac{V_{CH_4}}{V_{mol} . V_{water}} \tag{8}$$

The evaluation is essentially analogous for N_2O; however, the description of the drift behavior and the conversion to the concentration is more complex due to the nonlinearity behavior. Therefore, the concentration of N_2O was calculated by the following equation:

$$C_{N_2O} = \frac{\left(-b_{D;N} + \sqrt{\left(b_{D;N} \right)^2 - 4\, a_{D;N} \left(C_{D;N} - Area_{sample} \right)} \right)}{2\, a_{D;N} \left(V_{cal.loop} \, / \, V_{mol} . V_{water} \right)} \tag{9}$$

and the calculations of the drift behavior of a_D, b_D, and c_D followed the same procedure as that for CH_4

$$\text{i.e. } a_{D;N} = a_{N-1} + \frac{\left(a_E - a_B \right)}{N - 1} \tag{10}$$

2.4. Hydrographic Measurements

The temperature of in-situ surface water and salinity was taken from the ship's thermosalinograph (SEA-CAT SB 21 E, accuracy 0.01 °C, 0.001 S/m, resolution 0.001 °C, 0.0001 S/m) with its water inlet ~1.50 m below the waterline. Water samples from the Niskin bottles attached to the CTD rosette were also analyzed for temperature, salinity, and oxygen using a Seabird Electronics (SBE) 9 plus underwater unit. Nutrients were determined photometrically with a Skalar San++ Autoanalyzer following the procedures detailed in Grasshoff et al. (2009). The other hydrographic data, including wind speed (U_{10n}), air temperature, and ambient air pressure, were taken from the DSHIP data system.

In order to estimate the relative contributions of SACW and ESACW, we used the approach by Flohr (2014) with the water mass definitions by Mohrholz et al. (2008). In brief, we took the equations that define each of the two water masses based on potential temperature and salinity (T_p and S, respectively) as follows:

$$Tp_{ESACW} = 9.4454\, . S_{ESACW} - 319.03 \text{ and } Tp_{SACW} = 8.5607 . S_{SACW} - 289.08 \tag{11}$$

and transformed them to compute the corresponding contribution using a mass balance equation (with $a + b = 1$)

$$S_{Meas} = a . S_{SACW} + b . S_{ESACW} \tag{12}$$

whereby S_{Meas} equals measured salinity. The values were then multiplied by 100 to express the results in percentage (e.g., a contribution of 1 means that the contribution of a water mass on a certain location will be 100%). We purposefully limited the analysis to hydrographic data between 100 and 500 m to avoid the interference of nonconservative T/S behavior in upper waters and to cover the whole vertical range of SACW and ESACW along the shelf (Mohrholz et al., 2001).

2.5. Statistical Analysis

Statistical analysis and illustrations were performed with Microsoft Excel 2013, Ocean Data View (ODV4), MATLAB R2016a, and Minitab 17. Statistical differences were accepted as significant for a probability of <0.05 (i.e., $p < 0.05$).

Table 2

The Mean of Hydrographic Properties Including Temperature (°C), Salinity (PSU), Oxygen (μmol L⁻¹), Nitrate (NO₃⁻; μmol L⁻¹) and Density (kg m⁻³) Within the Angola-Gyre Type South Atlantic Central Water (SACW), SACW and Eastern-South Atlantic Central Water (ESACW) Between 100 and 500 m Depth

Hydrographic property	Angola-gyre type SACW (6°–12°S)	SACW (6°–12°S)	ESACW (south of 23°S)
Temperature (°C)	11.81 ± 1.37, 9.51–16.00	11.25 ± 1.70, 8.00–15.95	10.60 ± 1.26, 8.02–14.33
Salinity (PSU)	35.14 ± 0.16, 34.88–35.63	35.04 ± 0.19, 34.70–35.61	34.93 ± 0.13, 34.70–35.13
Oxygen (μmol L⁻¹)	34.20 ± 10.23, 20.30–60.90	54.92 ± 37.00, 14.05–182.67	84.72 ± 47.33, 14.06–220.74
Nitrate (NO₃⁻; μmol L⁻¹)	–	33.34 ± 4.42, 22.32–43.34	–
Density (kg m⁻³)	26.73 ± 0.14, 26.22–27.00	26.75 ± 0.17, 26.23–27.04	26.80 ± 0.13, 26.40–27.04

Note. Nitrate (NO₃⁻; μmol L⁻¹) is only available for SACW. The mean $\pm$ standard deviation ($\bar{x} \pm \sigma$) and the range are presented.

3. Results and Discussion

3.1. Hydrographic Properties

It is well documented that the along-shelf poleward undercurrent of SACW from the north is suppressed by strong cross-shelf circulation (Mohrholz et al., 2008), which results in a poleward decreasing SACW fraction (Siegfried et al., 2019). Earlier, Dingle and Nelson (1993) reported that poleward SACW intrusions display the lowest bottom oxygen concentrations (around 13 μmol L⁻¹) over the continental shelf between 20°S and Walvis Bay, while oxygen concentration increased southward and correlated with the intense ESACW intrusion in the area.

To analyze the dominant hydrographic properties (i.e., temperature, salinity, oxygen, and nitrate (NO₃⁻)) during this study, we divided the research area into three distinct subregions, including Angola-gyre type SACW (6°–12°S; after Mohrholz et al., 2008), SACW (12°–23°S; Dingle & Nelson, 1993), and ESACW (south of 23°S), irrespective of SS and WS surveys due to the differences in the geographical positions between the surveys with almost no overlap between the transects (Figure 1). The mean and standard deviation of the hydrographic properties in relation to dominant water mass in each subregion between 100 and 500 m depth is presented (Table 2).

The range of temperature and salinity in the Angola-gyre type SACW was within the range of 8.00–16.00°C and 34.72–35.63 PSU previously reported by Mohrholz et al. (2008). The mean oxygen concentration was about 34.00 μmol L⁻¹, also within the range of 22.43–68.48 μmol L⁻¹ in agreement to Mohrholz et al. (2008), except the lower limit of 20.30 μmol L⁻¹ in this study. In the other two regions i.e., 12°–23°S and south of 23°S, temperature and salinity declined while oxygen concentrations increased (Table 2).

The highest oxygen concentration ($\bar{x} \pm \sigma$: 84.72 $\pm$ 47.33 μmol L⁻¹; range: 14.06–220.74 μmol L⁻¹) was observed in the coldest waters of ESACW ($\bar{x} \pm \sigma$: 10.60 $\pm$ 1.26°C; range: 8.02–14.33°C) mostly during WS setting (Figure 1), while the lowest oxygen concentrations were determined in the regions hit by Angola-gyre type SACW with the mean of $\bar{x} \pm \sigma$: 34.20 $\pm$ 10.23 μmol L⁻¹ and within the range of 20.30–60.90 μmol L⁻¹. The oxygen concentration was also higher in SACW relative to Angola-gyre type SACW ($\bar{x} \pm \sigma$: 54.92 $\pm$ 37.00 μmol L⁻¹; range: 14.05–182.67 μmol L⁻¹) with the mean NO₃⁻ concentrations of $\bar{x} \pm \sigma$: 32.34 $\pm$ 4.42 μmol L⁻¹; range: 22.32–43.34 μmol L⁻¹ (Table 2). The zonal means of oxygen concentrations also revealed that well-oxygenated ESACW was dominant south of 23°S, although these well-oxygenated waters could still be detected at some stations further north.

We suggest a reduced southward intrusion of oxygen-depleted SACW into the northern Benguela at the time of sampling on both WS and SS, indicated by the mean oxygen concentration of $\bar{x} \pm \sigma$: 84.72 $\pm$ 47.33 μmol L⁻¹ in the south of 23°S, in contrast to lower mean oxygen concentration ($\bar{x} \pm \sigma$: 54.92 $\pm$ 37.00 μmol L⁻¹) due to a stronger imprint of SACW between 12° and 23°S (Table 2). A northward intrusion of ESACW with a higher oxygen content on the shelf might be dominant, driving ventilation over winter to springtime, potentially preventing the development of anoxic conditions in bottom waters (Mohrholz et al., 2008).
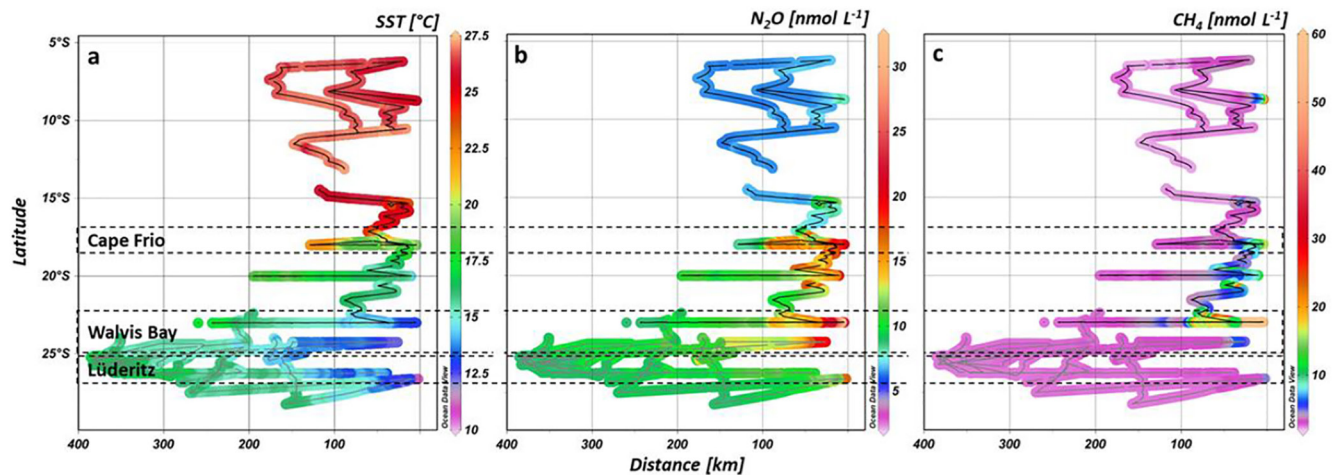
Figure 3. Surface profiles, plotted against distance from shore, of sea surface temperature (SST; a), nitrous oxide (N_2O; b), and methane (CH_4; c) on winter survey (WS; gray lines) and spring survey (SS; black lines). The range of the color scale of CH_4 profile is restricted between 0 and 60 (nmol L^{-1}) in order to obtain a reasonable resolution of the CH_4 distribution. The main upwelling cells include Cape Frio, Walvis Bay, and Lüderitz.

3.2. Regional Concentration Gradients of Surface N_2O and CH_4 Across the ESA

#### 3.2.1. Surface Observations of N_2O and CH_4

While N_2O and CH_4 distributions during WS and SS might not represent a complete picture of seasonal variability, they, however, provide a good indication of how the upwelling region of the ESA responds to synoptic variability of trace gases at the time of sampling. Overall, surface concentrations of N_2O and CH_4 showed similar distribution patterns, with the cold-water bands (10.00°C–15.00°C), in association with the local upwelling, extending offshore during both surveys and corresponding to maximum trace gas concentrations during the WS and the SS (Figure 3).

During both settings, SST evidenced the occurrence of upwelling in the vicinity of Walvis Bay and Lüderitz, with the lowest values of ~11.00 °C around Lüderitz. As shown exemplarily in Figure S1 in Supporting Information S1 a cross-shelf SST gradient was clearly evident, as a signature of upwelling events in the region. The SST ranged between 10.85°C and 27.40°C with the maxima observed north of 18°S whereas Lüderitz features the coldest SST across the nBUS, as also stated previously (Hutchings et al., 2009).

The most significant pattern of N_2O and CH_4 distribution is a steep cross-shelf gradient, with the highest concentrations in the vicinity of the upwelling cells, in agreement with the previous studies in the nBUS (Arévalo-Martínez et al., 2019) and in the entire BUS (e.g., Monteiro et al., 2006; Nevison et al., 2004). The gas concentrations ranged between ~6.00 and 31.80 nmol L^{-1} for N_2O and ~2.00 and 392.00 nmol L^{-1} for CH_4, with the maximal values at ca. 14.33°E and 23°S and 14.28°E and 23°S, respectively.

The maximal surface N_2O and CH_4 concentrations in the main ESA upwelling cells i.e., Cape Frio, Walvis Bay, and Lüderitz are found with a strong negative correlation with SST ($p < 0.05$, 95% confidence interval CI; Table S1 in Supporting Information S1).

The direct comparison between the two (WS and SS) settings was only possible between ~22°S and 23°S, where the ship's tracks overlapped, although the transits during WS proceeded further offshore (see Figure 1) but with fewer data points available relative to SS. The mean of N_2O and CH_4 concentrations for this zonal band were higher on the SS ($\bar{x} \pm \sigma$: ~13.00 ± 3.45 nmol L^{-1}; range: 8.73–31.80 nmol L^{-1} of N_2O and $\bar{x} \pm \sigma$: ~24.00 ± 64.35 nmol L^{-1}; range: 2.50–384.10 nmol L^{-1} of CH_4, $n = 1038$) in comparison with the WS ($\bar{x} \pm \sigma$: 9.70 ± 0.21 nmol L^{-1}; range: 9.22–10.04 nmol L^{-1} of N_2O, and $\bar{x} \pm \sigma$: ~2.54 ± 0.04 nmol L^{-1}; range: 2.50–2.60 nmol L^{-1} of CH_4, $n = 107$). Seasonal differences in N_2O and CH_4 concentrations derived by differences in the properties of the source waters during upwelling along with the large spatial and temporal variability of upwelling events (e.g., Morgan et al., 2019) makes it difficult to conclusively associate the observed differences to a seasonal component. On top of the synoptic variability, sea surface characteristics in the
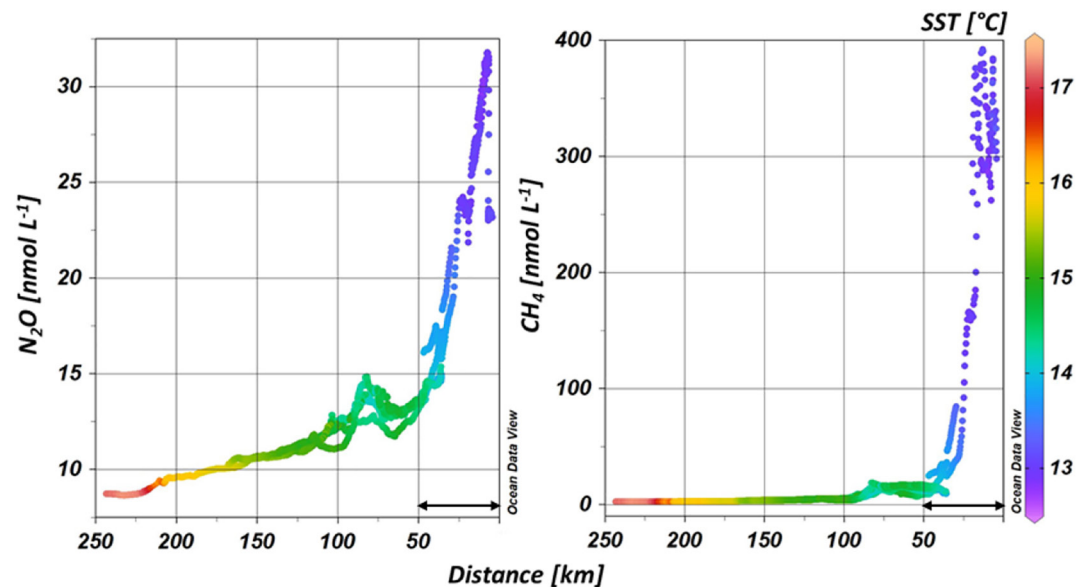
Figure 4. Inshore gradients of nitrous oxide (N$_2$O; left) and methane (CH$_4$; right) around Walvis Bay (23°S). The color bar represents sea surface temperature (SST). The arrows display the detailed study area.

Benguela region are known to be dominated by intraseasonal (eddy) variability (e.g., Mohrholz et al., 2014). Thus, despite comparable sampling locations, it seems unlikely that point observations can resolve the seasonal variability of N$_2$O and CH$_4$ concentrations in the nBUS. Future studies should base their efforts on experimental incubations and/or sustained observations in order to fully elucidate the seasonal variability.

To illustrate the upwelling-driven increase in surface N$_2$O and CH$_4$, the relationship between the surface gas concentrations and SST in the stations $\leq$ 50 km offshore around Walvis Bay is displayed in Figure 4.

Overall, both gases increased sharply close to the coast and markedly raised within 50 km offshore, with the strong CH$_4$ gradient occurring further inshore than the N$_2$O gradient.

The significant inverse correlation between the surface gas concentrations and SST (regression model; $p < 0.05$, 95% CI, $r^2 = 0.87$ (N$_2$O) and 0.84 (CH$_4$) and $n = 435$; Figure S2 in Supporting Information S1) represents the presence of cold, gas-enriched waters, upwelled to the surface, possibly due to advection/ mixing caused by upwelling events (e.g., Nevison et al., 2004). At few stations near the coast (total of 11 samples), the decline in N$_2$O and CH$_4$ concentrations was observed, while the mean temperature was $\bar{x} \pm \sigma$: 13.10 $\pm$ 0.11°C and not significantly different ($p > 0.05$) than at the adjacent stations ($x \geq 50$ km offshore). It is suggested that some other physical processes near the coast might have derived this decline but with only few data available in this study it is not possible to investigate it in more detail.

In general, surface waters were oversaturated with N$_2$O and CH$_4$ during our surveys ($\bar{x} \pm \sigma$: 119.00 $\pm$ 28.21%; range: 98.40–326.42% N$_2$O and $\bar{x} \pm \sigma$: 203.00 $\pm$ 770.00%; range: 100.61–15330.00% CH$_4$, respectively). The maximal N$_2$O and CH$_4$ saturation in the surface waters around the local upwelling cells (Figure S3 in Supporting Information S1) are explained by the influence of upwelled gas-enriched waters in agreement with other EBUS studies (e.g., Bange et al., 2001; Nevison et al., 2004). Extreme sea surface saturation of CH$_4$ around Walvis Bay during our surveys could also link to high sediment-derived CH$_4$ production in nutrient-enriched and less oxygenated coastal regions, including the mud-belt zone at ~23°S (Scranton & Farrington, 1997).

In general, N$_2$O and CH$_4$ flux densities across the ESA were mostly positive around the main upwelling cells at the time of sampling, indicating net outgassing of N$_2$O and CH$_4$ to the atmosphere (Figure S4 in Supporting Information S1). We computed highly variable sea-air N$_2$O flux densities of ($\bar{x} \pm \sigma$: 7.31 $\pm$ 14.70 μmol m^{-2} d^{-1}; range: −0.23–156.30 μmol m^{-2} d^{-1} of N$_2$O and $\bar{x} \pm \sigma$: 11.80 $\pm$ 103.20 μmol m^{-2} d^{-1}; range: 0.00–~3000.00 μmol m^{-2} d^{-1} of CH$_4$, $n = 29183$). These high fluctuations in the flux densities reflect

the spatial variability in SST and its interplay with N_2O and CH_4 concentrations at the surface waters (Figure 3). Although the range of N_2O flux densities lies almost within the range of 3.00–752.00 μmol m^{-2} d^{-1} reported for major hypoxic/suboxic and anoxic zones in the Eastern Tropical South Atlantic off Namibia, the maxima CH_4 flux was significantly higher than the reported upper limit, consistent with high spatial variability of CH_4 i.e., ~2.00 and 392.00 nmol L^{-1} in sea surface water (Arévalo-Martínez et al., 2019; Brüchert et al., 2009; Monteiro et al., 2006; Scranton & Farington, 1977).

The upwelling cells in the survey area are known as perennial hotspots for trace gas emissions to the atmosphere (Morgan et al., 2019), as the upwelled waters supercharged with N_2O and CH_4 reach the surface and result in strong outgassing. Profound meridional gradients in the gas fluxes were observed during this study; Cape Frio represented the greatest source of N_2O and CH_4 to the atmosphere ($\bar{x} \pm \sigma$: 48.10 $\pm$ 29.00 μmol m^{-2} d^{-1} of N_2O and $\bar{x} \pm \sigma$: 25.00 $\pm$ 28.30 μmol m^{-2} d^{-1} of CH_4) relative to Lüderitz ($\bar{x} \pm \sigma$: 2.00 $\pm$ 2.01 μmol m^{-2} d^{-1} of N_2O and $\bar{x} \pm \sigma$: 0.32 $\pm$ 0.30 μmol m^{-2} d^{-1} of CH_4). In agreement, Frame et al. (2014) also reported sea-air N_2O fluxes of 45.00 μmol m^{-2} d^{-1} around Cape Frio (i.e., 18°S).

The fluxes of N_2O and CH_4 in Walvis bay also showed the mean of $\bar{x} \pm \sigma$: 10.30 $\pm$ 14.12 μmol m^{-2} d^{-1} of N_2O and $\bar{x} \pm \sigma$: 36.00 $\pm$ 204.11 μmol m^{-2} d^{-1} of CH_4 respectively (Table S2 in Supporting Information S1) with the mean N_2O fluxes smaller than the flux range of 24.00–36.00 μmol m^{-2} d^{-1} reported by Gutknecht et al. (2013) for the region near 23°S between 13.2°E and 14.1°E in December 2009. Also, the sharp gradient in CH_4 fluxes around Walvis Bay might be associated with maximal sediment-derived CH_4 with possible sources of release including bubble transport and advective diffusion, transported to the surface waters by coastal upwelling, which results in a pronounced enhancement of the net flux of CH_4 to the atmosphere closer to the coast. Although the wind-driven transport is weaker in Walvis Bay relative to Cape Frio and Lüderitz, the shelf is wider and the mud-belt contains large amounts of organic material (Calvert & Price, 1983; Mollenhauer et al., 2007) which under low-oxygen conditions fosters intense cycling of trace gases in the area.

The elevated N_2O flux between 15°S and 25°S was also previously suggested in regions with upwelling-favorable wind stress curl (Chapman & Shannon, 1985). Shallow gas production, year-round upwelling-driven transport into the mixed layer and ventilation of older mesopelagic water along the coast were suggested as some other sources of high N_2O fluxes in the region (Frame et al., 2014).

To further explore the main drivers of N_2O and CH_4 fluxes across the ESA, the relations between the gas flux and SST, sea surface salinity (SSS), and wind speed was examined. The linear regression model with 95% CI was fitted to explore any significant correlation between the gas flux and the above variables (Table S3 in Supporting Information S1). The models represented significant inverse correlations between gas fluxes and SST and mostly SSS, whereas wind speed showed significant positive correlations with the gas flux in the regions ($p < 0.05$). However, the models fit best with wind speed and SST rather than SSS (i.e., higher r^2, Table S3 in Supporting Information S1).

3.2.2. Water Column Variability of N_2O and CH_4 Across the ESA

3.2.2.1. N_2O

The regional depth-cross sections of N_2O across the ESA (Figure 1) showed that it is mainly concentrated in the midlayers of the water column, in strong inverse correlation with oxygen concentrations ($p < 0.05$, $r^2 = 0.74$, $n = 644$; Figure 5).

Overall, N_2O ranged between 7.19 and ~50.00 nmol L^{-1} in both WS and SS with the maximal concentrations in midwater depth, while the core of N_2O-rich waters in the ESA is located at ~400 m depth. Our findings agree well with the maximal N_2O concentrations in depth between 200 and 400 m reported previously at the coastal stations of the northern transect (~10°–15°S; Frame et al., 2014) with the dominant SACW in the region. This finding is also in line with Oudot et al. (1990), Walter et al. (2004), and Arévalo-Martínez et al. (2017), who observed maximal N_2O concentrations in middle layers (150–500 m depth) of the tropical Atlantic. Resuspension of sediments around the continental shelf in the highly productive upwelling zone and/or aged oxygen-depleted SACW transported several kilometers away from the formation point (Mohrholz et al., 2008) was previously suggested to drive the high N_2O concentrations in the region (Frame et al., 2014). Also, shelf topography, like a marked steepness in the slope of the 11°S transect (Figure 5a
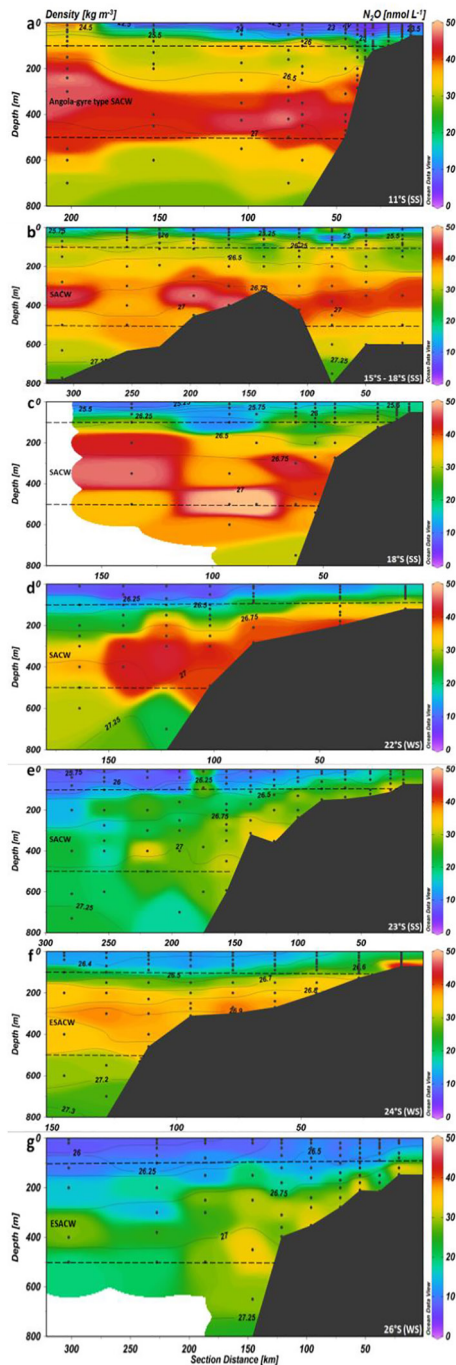
Figure 5. Depth-cross-shore profiles of N_2O concentration (color shading) with overlaid density in winter survey (WS) and spring survey (SS). From north to the south; (a) 11°S, (b) 15°–18°S, (c) 18°S; in the vicinity of Cape Frio, (d) 22°S, (e) 23°S; in the vicinity of Walvis Bay, (f) 24°S and (g) 26°S; in the vicinity of Lüderitz. The sampled stations used for gridding are marked by black circles. The dashed lines represent the regional dominant water masses between 100 and 500 m depth including Angola-gyre type South Atlantic Central Water (SACW), SACW, and Eastern-South Atlantic Central Water (ESACW). For the highest resolution, the lowermost boundary of the sampling is limited to 800 m depth.

and Hutchings et al., 2009), may facilitate N_2O-enriched waters to be upwelled in the presence of stronger winds, resulting in higher N_2O concentrations at shallow depth compared to other transects (Figure 5).

In the vicinity of the local upwelling cells, the maximal N_2O concentrations within the water column is found in Cape Frio and Walvis Bay with the mean of $\bar{x} \pm \sigma$: 26.00 ± 11.00 nmol L^{-1} and $\bar{x} \pm \sigma$: 24.43 ± 9.31 nmol L^{-1}, respectively, that are significantly higher (one-way ANOVA; $p < 0.05$, 95% CI) than Lüderitz ($\bar{x} \pm \sigma$: 18.00 ± 9.00 nmol L^{-1}).

Further analysis of the relationship between N_2O distribution and temperature-salinity profiles within the water column supports our earlier suggestion on a more pronounced ESACW during the WS due to the weakening of SACW intrusion, resulting in less N_2O concentration (Figure 6).

The correlation between ΔN_2O ($N_2O_{(observed)}$ - $N_2O_{(equilibrium)}$), apparent oxygen utilization (AOU; the difference between the equilibrated oxygen concentration and oxygen concentrations derived from in-situ data) and nitrate (NO_3^-) across the Cape Frio, Walvis Bay, and Lüderitz are evaluated (Figure 7).

The ΔN_2O/AOU slope indicates the amount of N_2O production per amount of oxygen consumed during organic matter (OM) remineralization. Since nitrification is closely linked to OM remineralization, higher slopes indicate higher oxygen consumption (i.e., higher AOU) and promoting N_2O production as the consequence. The relationship between ΔN_2O and NO_3^- also usually supports the evidence from ΔN_2O/AOU relationships since NO_3^- is the final product of OM remineralization (e.g., Elkins et al., 1978; Frame et al., 2014).

ΔN_2O/AOU slopes of 0.07, 0.08, and 0.09 of Cape Frio, Walvis Bay, and Lüderitz, respectively, for waters shallower than 800 m are in agreement with the slope of 0.08 reported by Arévalo-Martínez et al. (2017) for the tropical Atlantic Ocean and also similar to the values reported by Walter et al. (2006) for waters shallower than 500 m depth in the North Atlantic Ocean. Hence, based on the well-established knowledge of the above approach and the N_2O vertical profiles determined in this study (Figure 6), we infer that the observed N_2O maxima within the water column were produced by microbial nitrification in deeper waters. It is also noteworthy to point out that despite the difference in dominant subsurface water masses, the correlation between ΔN_2O and AOU is quite similar, representing N_2O production per unit of mineralization (or nitrification) stays constant and ΔN_2O/AOU slopes did not change significantly.

The lowest surface N_2O concentrations ($\bar{x} \pm \sigma$: 9.32 ± 0.90 nmol L^{-1}) were found in Lüderitz relative to Walvis Bay ($\bar{x} \pm \sigma$: 11.50 ± 3.00 nmol L^{-1}) and Cape Frio ($\bar{x} \pm \sigma$: 15.00 ± 3.35 nmol L^{-1}). Lüderitz is also characterized by strong winds, high offshore advection, and strong turbulent mixing (e.g., Hutchings et al., 2009). Arévalo-Martínez et al. (2019) hypothesized that the low surface N_2O concentrations in Lüderitz with respect to Walvis Bay or Cape Frio, could be due to reduced supply of organic matter, increased influence of the ESACW or a combination of both. However, this was concluded based on surface measurements only and without any data from the underlying waters. From the vertical sections, it would appear that, at least for the time of sampling during this study,
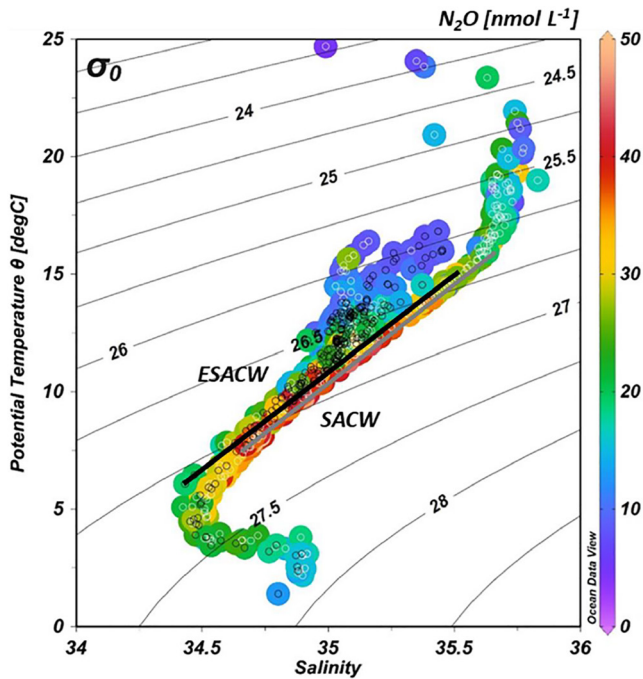
Figure 6. Temperature-salinity (*T/S*) plot in relation to N$_2$O concentration between sea surface and 800 m depth. Winter setting (WS) and spring setting (SS) are marked by black and white circles, respectively. The two end members mixing lines for SACW and ESACW are represented by light gray and black solid lines respectively. Isopycnals are displayed by gray solid lines.

the high concentrations of N$_2$O remained close to the bottom, creating an N$_2$O pool in isolation from vertical transport to the surface resulting in lower surface concentrations.

The lower slope of regression for the calculated $\Delta N_2O/NO_3^-$ as the transects proceeded southward (Figure 7) were lower than 0.56 reported by Arévalo-Martínez et al. (2017) but might indicate mixing of waters with different N$_2$O concentrations during the time of sampling in Walvis Bay.

In order to investigate the contribution of SACW and ESACW to the observed distribution in N$_2$O concentrations, the percentage of each water mass was calculated as in Flohr (2014). In brief, the water mass contribution (in %) at each depth for each profile was computed (see Equations 11 and 12, Section 2.4), hence, each line represents an integrated profile over the corresponding latitude (Figure 8).

We found that SACW was dominant off Cape Frio with ~92.50% relative to only 7.50% of ESACW, while ESACW was mostly dominant in Walvis Bay and Lüderitz with 70.00% and 78.00%, respectively (Figure 8). The ATZ (i.e., 6°–14°S, Figure 1) also contained ~97.00% SACW relative to only ~3.00% of ESACW. Based on the relationship between the spatial distribution of N$_2$O and the dominant regional water masses, we suggest that the distribution pattern of N$_2$O in the surface waters around Lüderitz was influenced by oxygen-rich ESACW that dominate the water mass composition relative to aged SACW in the deeper layers over the shelf (Figure 5). In line with our assumption, most of SACW off the northern Namibia is advected away from the shelf but partly remains in bottom layers during the winter season (Mohrholz et al., 2008). However, the entire water column might also be influenced by meridional flows and enhanced cross-shelf circulation during the upwelling season (Mohrholz et al., 2008).
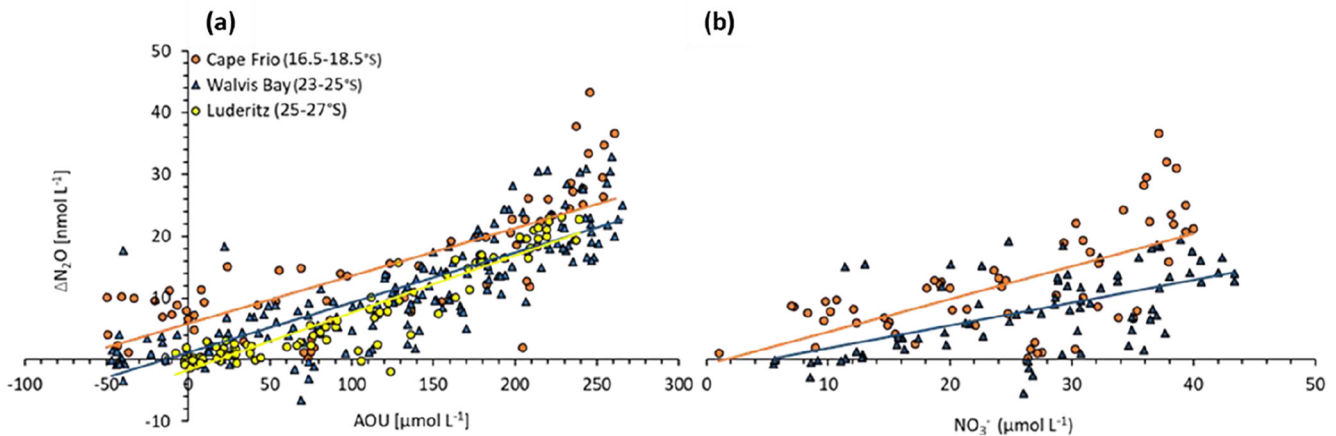
Figure 7. $\Delta N_2O/AOU$ and $\Delta N_2O/NO_3^-$ correlations in Cape Frio, Walvis Bay, and Lüderitz (for the latter, only $\Delta N_2O/AOU$ is available). The regression lines of $\Delta N_2O/AOU$ in Cape Frio ($\Delta N_2O = 0.07$ (AOU) + 5.88, $r^2 = 0.60$, $n = 68$), Walvis Bay ($\Delta N_2O = 0.08$ (AOU) + 1.16, $r^2 = 0.70$, $n = 167$), and Lüderitz ($\Delta N_2O = 0.09$ (AOU) − 1.71, $r^2 = 0.87$, $n = 89$) are displayed by orange, blue, and yellow line in panel (a), respectively. The regression lines of $\Delta N_2O/NO_3^-$ in panel (b) are including orange line ($\Delta N_2O = 0.63$ (NO$_3^-$) − 1.01, $r^2 = 0.40$, $n = 59$) of Cape Frio and blue line ($\Delta N_2O = 0.43$ (NO$_3^-$) − 2.14, $r^2 = 0.33$, $n = 79$) of Walvis Bay.
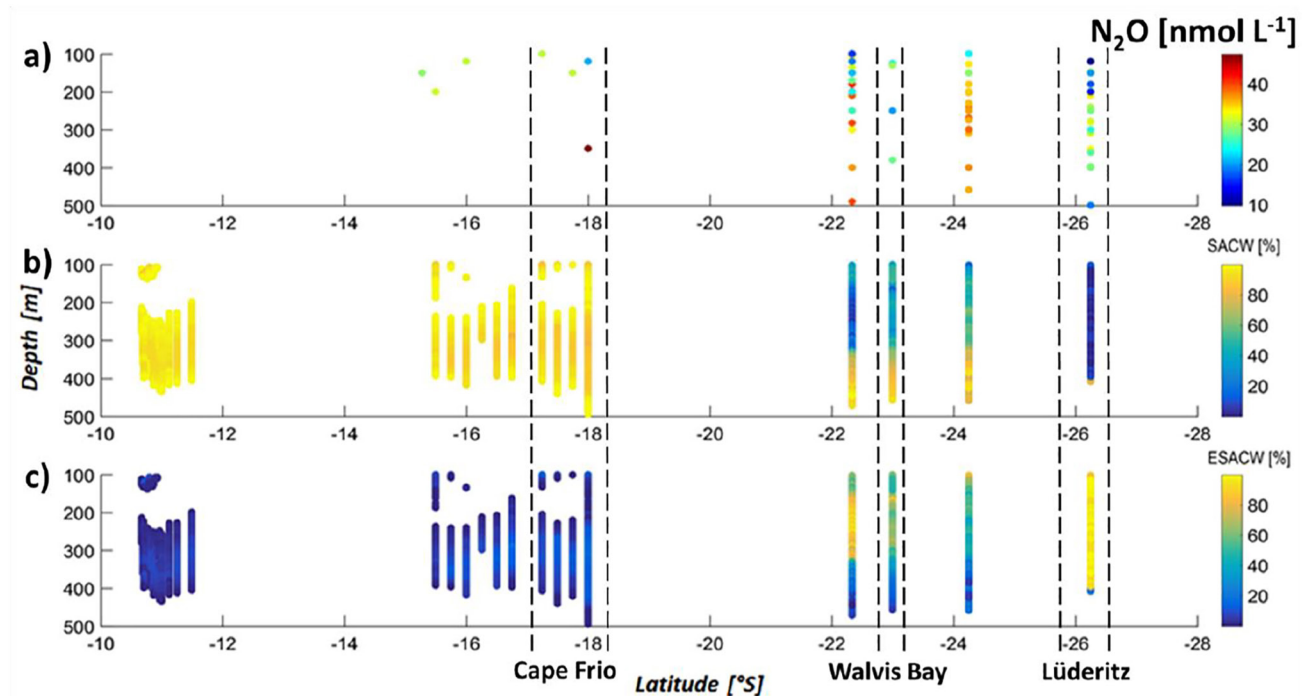
Figure 8. Meridional distribution of water column N_2O (a) and the corresponding SACW (b) and ESACW (c) percentages between 100 and 500 m depth.

3.2.2.2. CH_4

The vertical distribution of CH_4 revealed a heterogeneous pattern with sharp cross-shelf gradients and the highest concentrations being associated with waters near to the sediment. CH_4 concentrations varied between 0.35 and extreme 346.53 nmol L^{-1} during SS (Figure 9).

The vertical advection of CH_4 from sedimentary sources to the surface layer associated with upwelling in shallow coastal sections might shorten the time available for microbial oxidation processes in the water column (e.g., Reeburgh, 2007; Rehder et al., 1999) resulting in the observed high maintained CH_4 concentration over the continental shelf (Figure 9). This statement is also further supported by recorded maximal CH_4 concentrations within the entire water column at 23°S in the vicinity of Walvis Bay, associated with shallow water depths and an extremely organic-rich underlying diatomaceous mud-belt (van der Plas et al., 2007), serving as a substrate for CH_4 production and sustaining the water column CH_4 maxima. These pronounced concentrations were not surprising as Scranton and Farrington (1977) recorded CH_4 concentrations as high as 879.00 nmol L^{-1} within the water column off Walvis Bay in the austral summer but with small upwelling and sulphidic conditions over the inner shelf. CH_4 disequilibrium with the atmosphere (i.e., ΔCH_4) was also reported to a maximum of ~1500.00 nmol L^{-1} in the very shallow waters for nearshore ecosystems using machine-learning models to map the global oceanic surface distribution of CH_4 disequilibrium (Weber et al., 2019). In other transects, high CH_4 concentrations were also found in the bottom waters directly overlying the sediments (Figure 10), consistent with previous observations by Brüchert et al. (2009) on the central Namibian shelf, who suggested episodic advection and release of CH_4 from sediments due to gas bubble transport to the overlying waters. Based on the good correlation between gas distribution and SST, the transition of the sedimentary derived CH_4, independent of a bubble-mediated or diffusive transport across the sediment-water interface, to the upper water layers is clearly facilitated by upwelling.

High CH_4 concentration near the sediment, with sulfate almost depleted in the sediment, is suggested to favor CH_4 production through methanogenesis and/or microbial production from CO_2 or acetate (Reeburgh, 2007). However, no clear pattern of CH_4 distributions within the water column was evident during both WS and SS, and few local higher concentrations of CH_4 in the upper water might be associated with in-situ CH_4 production (Holmes et al., 2000; Schmale et al., 2010, 2018). CTD-derived fluorescence data (au) in upper 100 m depth, an indicator of primary productivity also revealed the regions with higher
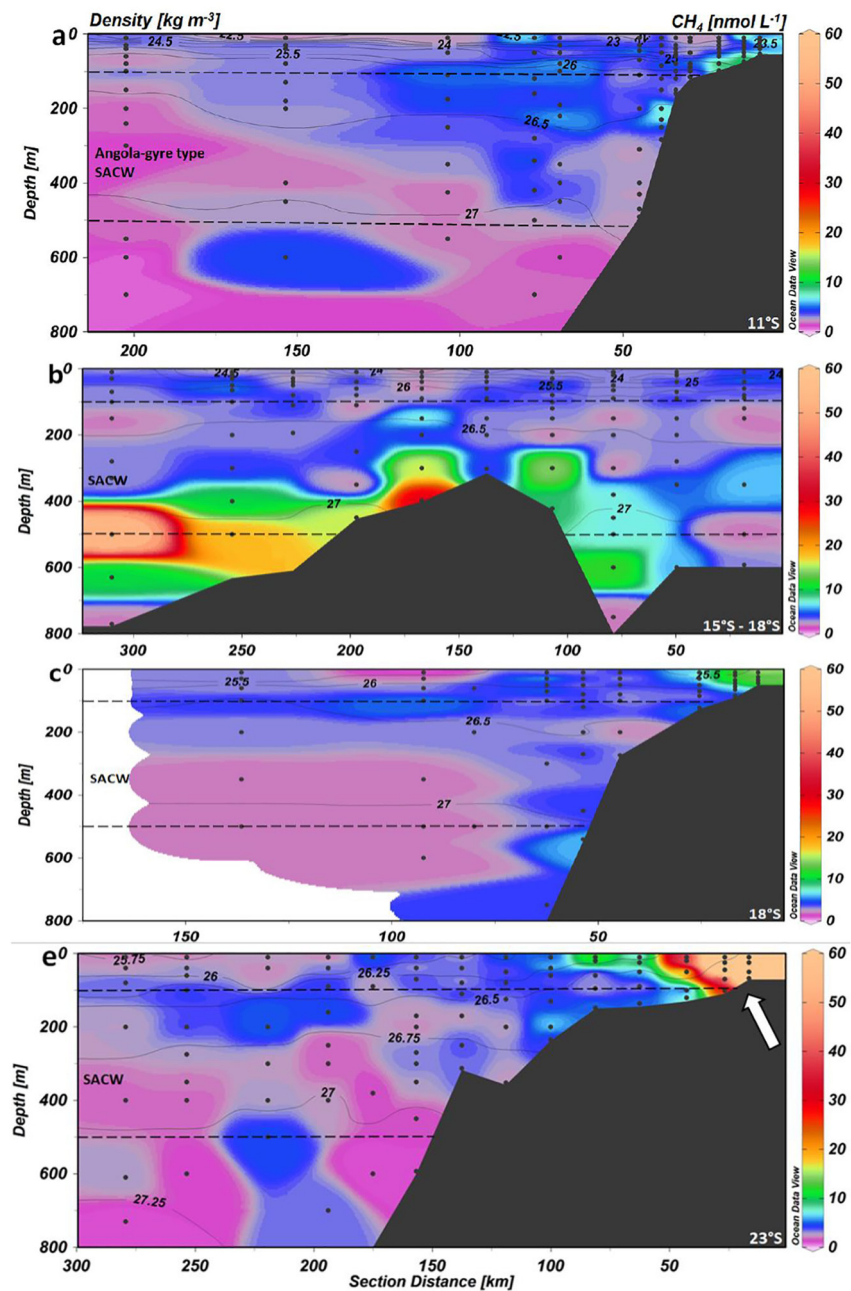
Figure 9. The regional depth-cross sections of CH_4 across the ESA in spring setting (SS); from North to the South; (a) 11°S, (b) 15°–18°S, (c) 18°S; in the vicinity of Cape Frio and (e) 23°S; in the vicinity of Walvis Bay. Solid circles show the location of actual measurements. Density overlaid contours are displayed with gray lines. The range of the color scale is restricted to 0–60 (nmol L^{-1}) in order to obtain a reasonable resolution of the CH_4 distribution. The region with maxima CH_4 concentration (~350 nmol L^{-1}) is displayed by a white arrow in plot (e). The dashed lines represent the regional dominant water masses between 100 and 500 m depth including Angola-gyre type South Atlantic Central Water (SACW) and SACW. The lowermost boundary of the samples is 800 m depth.

fluorescence signals in match with those local CH_4 hotspots in the oxygenated layer during SS setting (Figure S5 in Supporting Information S1).

Also, a further assessment of the influence of the water masses implying its hydrographic characteristics (i.e., temperature and salinity) on CH_4 distributions revealed no direct water mass control on CH_4 gradients, while some regional hotspots mainly in the vicinity of Cape Frio and Walvis Bay are present (Figure 10).
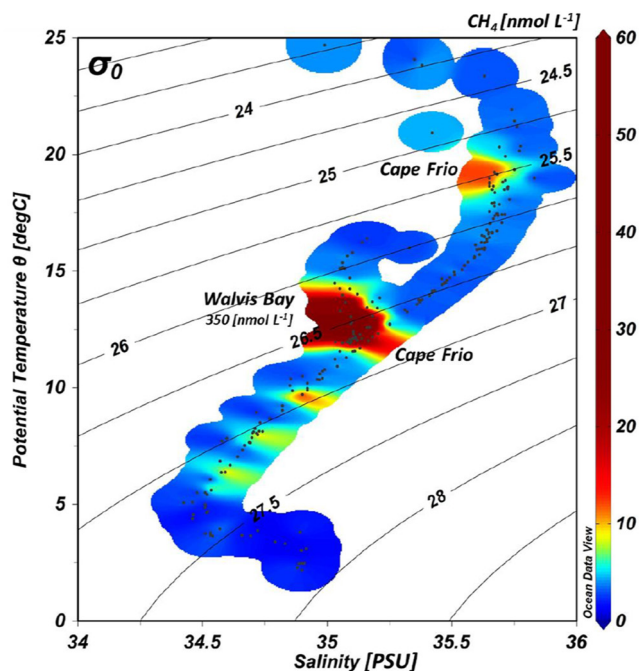
Figure 10. Temperature-salinity (*T/S*)-CH$_4$ between surface and 800 m depth during spring setting (SS). Isopycnals are displayed by solid lines. The range of the color scale was restricted to 0–60 (nmol L^{-1}) in order to obtain a reasonable resolution of the CH$_4$ distribution.

Regional hotspots of CH$_4$ might be the result of some local productions that have been advected to the surface via local upwelling. Besides, subsurface moderate CH$_4$ concentrations ~5.00 nmol L^{-1} can be maintained by lateral mixing/advection of CH$_4$-enriched water and/or the loss of CH$_4$ from the surface layers through outgassing to the atmosphere (Naqvi et al., 2010). Also, CH$_4$ enrichment in the oxygenated upper water column associated with methanogenic bacteria and archaea (Holmes et al., 2000; Schmale et al., 2010, 2018), in-situ anoxic CH$_4$ production in subsurface layers, just below the mixed layer, linked to primary productivity and biogenic materials such as zooplankton fecal pellets can contribute to sub-thermocline CH$_4$ enrichment (Oremland, 1979; Reeburgh, 2007).

CH$_4$ depletion in subsurface waters in line with earlier reports (Brüchert et al., 2009; Scranton & Farrington, 1977) suggests CH$_4$ consumption via oxidative loss through the water column (Rehder et al., 1999) but with less evidence of advection of low CH$_4$ waters (Naqvi et al., 2010; Schmale et al., 2018).

In summary, it seems that the CH$_4$ accumulation in deep shelf waters is the consequence of bottom release, whereas the low concentrations in the surface are most likely due to CH$_4$ loss via oxidation or air-sea gas transfer, while there was no clear evidence of the advection of low CH$_4$ waters transported by dominant water masses. It is suggested that two sources of CH$_4$ within the water column in the ESA might be present; a sedimentary source with restricted diffusive flux to the upper layers and restricted efflux to the atmosphere as the consequence, due to possible CH$_4$ consumption, and an upper source of in-situ biogenic production of CH$_4$ by bacteria within the oxygenated layer with greater impact on atmospheric CH$_4$ flux. The hot spots of CH$_4$ in both the surface survey and hydrographic sections are clearly related to sedimentary sources (Figures 3 and 9). This may indicate that CH$_4$ is mainly derived from the sedimentary methanogenesis near the shelf while N$_2$O distribution is more likely linked to water mass distribution (see Section 3.2.2.1).

3.3. Controls on the Distribution and Flux Patterns of N$_2$O and CH$_4$ Derived From Surface Data and Hydrographic Sections

We found that the concentration gradients of N$_2$O and CH$_4$ are very similar both meridionally and zonally; however, the extent of the differences between the high-end and low-end members of the concentrations/saturations range is different. This argues in favor of a pronounced effect of local sources for CH$_4$ than N$_2$O in the region in particular where the shelf is the broadest (off Walvis Bay). Concerning N$_2$O on the other hand, low-oxygen waters from the poleward undercurrent impinge in the shelf close to Cape Frio and often result in concentrations higher than off Walvis Bay itself not because N$_2$O concentrations are necessarily higher in Cape Frio but due to shelf topography (Figure 5) that makes it easier for these waters to be upwelled in the presence of stronger winds (Arévalo-Martínez et al., 2019; Frame et al., 2014).

The surface sections revealed that both trace gases increase with lower SST, showing the effect of upwelling on trace gas emission, but with CH$_4$ enrichment more pronounced to the inner shelf, also present in the vertical profiles (Figures 9c and 9e). As revealed here, this is mainly related to the fact that the source of the two trace gases is different; large-scale accumulation of N$_2$O in midwaters due to nitrification, correlating with AOU, and resulting in a clear relation to the water mass diagram whereas regional release from organic-rich sediments, leading to shelf-near plumes and locally restricted spots of high CH$_4$ (Figure 10).

4. Conclusions

N_2O and CH_4 flux densities across the ESA were mostly positive at the time of sampling, indicating the net outgassing of N_2O and CH_4 to the atmosphere. Profound meridional gradient in the gas fluxes was found, while Cape Frio represented the greatest source of N_2O and CH_4 to the atmosphere relative to Lüderitz. The sharp gradient in CH_4 fluxes in Walvis Bay associated with intense sediment-derived CH_4, result in a pronounced enhancement of the net flux of CH_4.

We suggest that the spatial variability on the dominant water masses on the shelf and its topography, as well as the coincidence with upwelling events, play a major role on the production and advection of N_2O toward the near surface; ultimately controlling the extent of the sea-air fluxes in the region. We suggest a poleward undercurrent of SACW in conjunction with shelf topography and possible local production result in more efficiently upwelled N_2O in Cape Frio than off Walvis Bay irrespective of the higher gas concentrations in Walvis Bay. Concerning CH_4, however, no clear evidence of the advection of low CH_4 waters transported by dominant water masses was found while profound local sources for CH_4 in particular off Walvis Bay are suggested.

The comparison of the identification of high N_2O and CH_4 concentrations in a T/S diagram (Figures 6 and 10) and the observation of the more inshore concentrated hot spots of CH_4 (e.g., Figure 4) reveal the marked difference in the controlling factors for their emission to the atmosphere. While the upwelling-induced transport of enriched subsurface waters to the surface is required for both gases, the subsurface enrichment of N_2O is governed by large-scale water mass properties and their distribution, while high CH_4 concentrations are mostly governed by local sedimentary sources.

The projected intensification of upwelling-favorable winds as well as increased deoxygenation might increase the extent of subsurface N_2O-enriched and CH_4-enriched waters and their effective transport toward the surface, potentially increasing the atmospheric greenhouse gas source as a consequence of coastal upwelling (Sydeman et al., 2014). Hence, the interplay between these changes and future ocean warming-driven changes in the large-scale circulation of the ESA will determine the role of this region for the global budget of the gases. In this framework, the focus of future observational programs should be set on sustained, fixed-point measurements which adequately resolve trace gases trends in intraseasonal and interannual time scales based on intercomparable methodology (Wilson et al., 2018, 2020).

Data Availability Statement

All the data are available to download at PANGAEA Data Publisher for Earth and Environmental Science at https://doi.org/10.1594/PANGAEA.936689.

References

Arévalo-Martínez, D. L., Beyer, M., Krumbholz, M., Piller, I., Kock, A., Steinhoff, T., et al. (2013). A new method for continuous measurements of oceanic and atmospheric N_2O, CO and CO_2: Performance of off-axis-integrated cavity output spectroscopy (OA-ICOS) coupled to non-dispersive infrared detection (NDIR). *Ocean Science*, 9, 1071–1087.

Arévalo-Martínez, D. L., Kock, A., Steinhoff, T., Brandt, P., Dengler, M., Fischer, T., et al. (2017). Nitrous oxide during the onset of the Atlantic cold tongue. *Journal of Geophysical Research: Oceans*, 122, 171–184. https://doi.org/10.1002/2016JC012238

Arévalo-Martínez, D. L., Steinhoff, T., Brandt, P., Körtzinger, A., Lamont, T., Rehder, G., & Bange, H. W. (2019). N_2O emissions from the northern Benguela upwelling system. *Geophysical Research Letters*, 46, 3317–3326. https://doi.org/10.1029/2018GL081648

Baer, D. S., Paul, J. B., Gupta, M., & O'Keefe, A. (2002). Sensitive absorption measurements in the near infrared region using off-axis integrated-cavity-output spectroscopy. *Applied Physics B: Lasers and Optics*, 75(2), 261–265. https://doi.org/10.1007/s00340-002-0971-z

Bakker, D. C., Bange, H. W., Gruber, N., Johannessen, T., Upstill-Goddard, R. C., Borges, A. V., et al. (2014). Air-sea interactions of natural long-lived greenhouse gases (CO_2, N_2O, CH_4) in a changing climate. *Ocean-Atmosphere Interactions of Gases and Particles*, 133–169.

Bakun, A. (2017). Climate, change and ocean deoxygenation within intensified surface-driven upwelling, circulations. *Philosophical Transactions of the Royal Society A*, 375, 20160327. https://doi.org/10.1098/rsta.2016.0327

Bakun, A., Field, D. B., Redondo-rodriguez, A., & Weeks, S. J. (2010). Greenhouse gas, upwelling-favorable winds, and the future of coastal ocean upwelling ecosystems. *Global Change Biology*, 16, 1213–1228. https://doi.org/10.1111/j.1365-2486.2009.02094.x

Bange, H. W., Andreae, M. O., Lal, S., Law, C. S., Naqvi, S. W. A., Patra, P. K., et al. (2001). Nitrous oxide emissions from the Arabian Sea: A synthesis. *Atmospheric Chemistry and Physics*, 1, 61–71. https://doi.org/10.5194/acp-1-61-2001

Bates, T. S., Kelly, K. C., Johnson, J. E., & Gammon, R. H. (1996). A reevaluation of the open ocean source of methane to the atmosphere. *Journal of Geophysical Research*, 101, 6953–6961. https://doi.org/10.1029/95JD03348

Boetius, A., Ravenschlag, K., Schubert, C. J., Rickert, D., Widdel, F., Gieseke, A., et al. (2000). A marine microbial consortium apparently mediating anaerobic oxidation of methane. *Nature*, 407(6804), 623–626. https://doi.org/10.1038/35036572

Boyer, T. P., Antonov, J. I., Baranova, O. K., Coleman, C., Garcia, H. E., Grodsky, A., et al. (2013). *World ocean database 2013, NOAA Atlas NESDIS 72*. Silver Spring. https://doi.org/10.7289/V5NZ85MT

Brüchert, V., Currie, B., & Peard, K. R. (2009). Hydrogen sulphide and methane emissions on the central Namibian shelf. *Progress in Oceanography*, *83*, 169–179. https://doi.org/10.1016/j.pocean.2009.07.017

Calvert, S. E., & Price, N. B. (1983). Geochemistry of Namibian shelf sediments. In E. Suess, & J. Thiede (Eds.), *Coastal upwelling its sediment record. NATO Conference Series (IV marine sciences)* (Vol. *10B*, pp. 337–375). Springer. https://doi.org/10.1007/978-1-4615-6651-9_17

Cantera, J. J. L., & Stein, L. Y. (2007). Role of nitrite reductase in the ammonia-oxidizing pathway of *Nitrosomonas europaea*. *Archives of Microbiology*, *188*(4), 349–354. https://doi.org/10.1007/s00203-007-0255-4

Capone, D. G., & Hutchins, D. A. (2013). Microbial biogeochemistry of coastal upwelling regimes in a changing ocean. *Nature Geoscience*, *6*(9), 711–717. https://doi.org/10.1038/ngeo1916

Chapman, P., & Shannon, L.V. (1985). The Benguela ecosystem Part II. Chemistry and related processes. *Oceanography and Marine Biology: An Annual Review*, *23*, 183–251.

Charpentier, J., Farias, L., & Pizarro, O. (2010). Nitrous oxide fluxes in the central and eastern South Pacific. *Global Biogeochemical Cycles*, *24*, GB3011. https://doi.org/10.1029/2008GB003388

Ciais, P., Sabine, C., Bala, G., Bopp, L., Brovkin, V., Canadell, J., et al. (2013). Climate change 2013. The physical science basis. In K. M. Tignor, S. K. Allen, J. Boschung, A. Nauels, Y. Xia, V. Bex, & P. M. Midgley (Eds.), *Contribution of working group I to the fifth assessment report of the intergovernmental panel on climate change* (pp. 465–570).

Dingle, R. V., & Nelson, G. (1993). Sea-bottom temperature, salinity and dissolved oxygen on the continental margin off South-Western Africa. *South African Journal of Marine Science*, *13*, 33–49. https://doi.org/10.2989/025776193784287220

Elkins, J. W., Wofsy, S., McElroy, M. B., Kolb, C. E., & Kaplan, W. A. (1978). Aquatic sources and sinks for nitrous oxide. *Nature*, *275*, 602–606. https://doi.org/10.1038/275602a0

Flohr, A. (2014). *Carbon pumps in the Benguela current upwelling system (Doctoral dissertation)*. Staats-und Universitätsbibliothek Hamburg Carl von Ossietzky.

Frame, C., Deal, E., Nevison, C. D., & Casciotti, K. L. (2014). N_2O production in the eastern South Atlantic: Analysis of N_2O stable isotopic and concentration data. *Global Biogeochemical Cycles*, *28*, 1262–1278. https://doi.org/10.1002/2013GB004790

Friedrichs, G., Bock, J., Temps, F., Fietzek, P., Körtzinger, A., & Wallace, D. W. (2010). Toward continuous monitoring of seawater $^{13}CO_2$/$^{12}CO_2$ isotope ratio and pCO_2: Performance of cavity ringdown spectroscopy and gas matrix effects. *Limnology and Oceanography: Methods*, *8*(10), 539–551. https://doi.org/10.4319/lom.2010.8.539

Grasshoff, K., Kremling, K., & Ehrhardt, M. (2009). *Methods of seawater analysis*. John Wiley & Sons.

Gülzow, W., Rehder, G., Schneider, B., Deimling, J. S. V., & Sadkowiak, B. (2011). A new method for continuous measurement of methane and carbon dioxide in surface waters using off-axis integrated cavity output spectroscopy (ICOS): An example from the Baltic Sea. *Limnology and Oceanography: Methods*, *9*(5), 176–184. https://doi.org/10.4319/lom.2011.9.176

Gutknecht, E., Dadou, I., Le Vu, B., Cambon, G., Sudre, J., Garçon, V., et al. (2013). Coupled physical/biogeochemical modeling including O_2-dependent processes in the Eastern Boundary upwelling systems: Application in the Benguela. *Biogeosciences*, *10*, 3559–3591. https://doi.org/10.5194/bg-10-3559-2013

Holmes, M. E., Sansone, F. J., Rust, T. M., & Popp, B. N. (2000). Methane production, consumption, and air-sea exchange in the open ocean. *Global Biogeochemical Cycles*, *14*, 1–10. https://doi.org/10.1029/1999GB001209

Hutchings, L., van der Lingen, C. D., Shannon, L. J., Crawford, R. J. M., Verheye, H. M. S., Bartholomae, C. H., et al. (2009). The Benguela current: An ecosystem of four components. *Progress in Oceanography*, *83*, 15–32. https://doi.org/10.1016/j.pocean.2009.07.046

Johnson, J. E. (1999). Evaluation of a seawater equilibrator for shipboard analysis of dissolved oceanic trace gases. *Analytica Chimica Acta*, *395*(1–2), 119–132. https://doi.org/10.1016/s0003-2670(99)00361-x

Klintzsch, T., Langer, G., Nehrke, G., Wieland, A., Lenhart, K., & Keppler, F. (2019). Methane production by three widespread marine phytoplankton species: Release rates, precursor compounds, and potential relevance for the environment. *Biogeosciences*, *16*(20), 4129–4144. https://doi.org/10.5194/bg-16-4129-2019

Knittel, K., & Boetius, A. (2009). Anaerobic oxidation of methane: Progress with an unknown process. *Annual Review of Microbiology*, *63*, 311–334. https://doi.org/10.1146/annurev.micro.61.080706.093130

Körtzinger, A., Thomas, H., Schneider, B., Gronau, N., Mintrop, L., & Duinker, J. C. (1996). At-sea intercomparison of two newly designed underway pCO_2 systems—Encouraging results. *Marine Chemistry*, *52*, 133–145.

Large, W., & Pond, S. (1982). Sensible and latent heat flux measurements over the ocean. *Journal of Physical Oceanography*, *12*, 464–482. https://doi.org/10.1175/1520-0485(1982)012<0464:salhfm>2.0.co;2

Löscher, C. R., Kock, A., Könneke, M., LaRoche, J., Bange, H. W., & Schmitz, R. A. (2012). Production of oceanic nitrous oxide by ammonia-oxidizing archaea. *Biogeosciences*, *9*(7), 2419–2429. https://doi.org/10.5194/bg-9-2419-2012

Lueker, T. J., Walker, S. J., Vollmer, M. K., Keeling, R. F., Nevison, C. D., Weiss, R. F., & Garcia, H. E. (2003). Coastal upwelling air-sea fluxes revealed in atmospheric observations of O_2/N_2, CO_2 and N_2O. *Geophysical Research Letters*, *30*(6), 1292. https://doi.org/10.1029/2002GL016615

Middelburg, J. J., Klaver, G., Nieuwenhuize, J., Wielemaker, A., de Haas, W., Vlug, T., & van der Nat, J. F. (1996). Organic matter mineralization in intertidal sediments along an estuarine gradient. *Marine Ecology Progress Series*, *132*, 157–168. https://doi.org/10.3354/meps132157

Mohrholz, V., Bartholomae, C. H., Van der Plas, A. K., & Lass, H. U. (2008). The seasonal variability of the northern Benguela undercurrent and its relation to the oxygen budget on the shelf. *Continental Shelf Research*, *28*(3), 424–441. https://doi.org/10.1016/j.csr.2007.10.001

Mohrholz, V., Eggert, A., Junker, T., Nausch, G., Ohde, T., & Schmidt, M. (2014). Cross shelf hydrographic and hydrochemical conditions and their short term variability at the northern Benguela during a normal upwelling season. *Marine Systems*, *140*, 92–110. https://doi.org/10.1016/j.jmarsys.2014.04.019

Mohrholz, V., Schmidt, M., & Lutjeharms, J. R. E. (2001). The hydrography and dynamics of the Angola-Benguela frontal zone and environment in April 1999. *South African Journal of Science*, *97*, 199–208.

Mollenhauer, G., Inthorn, M., Vogt, T., Zabel, M., Sinninghe Damsté, J. S., & Eglinton, T. I. (2007). Aging of marine organic matter during cross-shelf lateral transport in the Benguela upwelling system revealed by compound-specific radiocarbon dating. *Geochemistry, Geophysics, Geosystems*, *8*, Q09004. https://doi.org/10.1029/2007GC001603

Monteiro, P. M. S., Van der Plas, A., Mohrholz, V., Mabille, E., Pascall, A., & Joubert, W. (2006). Variability of natural hypoxia and methane in a coastal upwelling system: Oceanic physics or shelf biology? *Geophysical Research Letters*, *33*, L16614. https://doi.org/10.1029/2006GL026234

Monteiro, P. M. S., Van Der Plas, A. K., Melice, J. L., & Florenchie, P. (2008). Interannual hypoxia variability in a coastal upwelling system: Ocean-shelf exchange, climate and ecosystem-state implications. *Deep Sea Research Part I: Oceanographic Research Papers*, *55*(4), 435–450. https://doi.org/10.1016/j.dsr.2007.12.010

Morgan, E., Lavrič, J. V., Arévalo-Martínez, D. L., Bange, H. W., Steinhoff, T., Seifert, T., & Heimann, M. (2019). Air-sea fluxes of greenhouse gases and oxygen in the northern Benguela current region during upwelling events. *Biogeosciences*, *16*(20), 4065–4084. https://doi.org/10.5194/bg-16-4065-2019

Myhre, G. D. (2013). Anthropogenic and natural radiative forcing. Cambridge United Kingdom and New York NY USA: Climate Change. In *The physical science basis. Contribution of working group I to the fifth assessment report of the intergovernmental panel on climate change* (pp. 129–234).

Naqvi, S. W. A., Bange, H. W., Farías, L., Monteiro, P. M. S., Scranton, M. I., & Zhang, J. (2010). Marine hypoxia/anoxia as a source of CH_4 and N_2O. *Biogeosciences*, *7*, 2159–2190.

Nevison, C. D., Lueker, T. J., & Weiss, R. F. (2004). Quantifying the nitrous oxide source from coastal upwelling. *Global Biogeochemical Cycles*, *18*, GB1018. https://doi.org/10.1029/2003GB002110

Nevison, C. D., Weiss, R. F., & Erickson, D. J., III. (1995). Global oceanic emissions of nitrous oxide. *Journal of Geophysical Research*, *100*, 15809–15820. https://doi.org/10.1029/95JC00684

Oremland, R. S. (1979). Methanogenic activity in plankton samples and fish intestines—Mechanism for in situ methanogenesis in oceanic surface waters. *Limnology and Oceanography*, *24*, 1136–1141. https://doi.org/10.4319/lo.1979.24.6.1136

Oudot, C., Andrie, C., & Montel, Y. (1990). Nitrous oxide production in the tropical Atlantic Ocean. *Deep-Sea Research*, *37*, 183–202. https://doi.org/10.1016/0198-0149(90)90123-d

Reeburgh, W. S. (2007). Oceanic methane biogeochemistry. *Chemical Reviews*, *107*(2), 486–513. https://doi.org/10.1021/cr050362v

Rehder, G., Keir, R. S., Suess, E., & Rhein, M. (1999). Methane in the northern Atlantic controlled by microbial oxidation and atmospheric history. *Geophysical Research Letters*, *26*, 587–590. https://doi.org/10.1029/1999GL900049

Ritchie, G. A. F., & Nicholas, D. J. D. (1972). Identification of the sources of nitrous oxide produced by oxidative and reductive processes in *Nitrosomonas europaea*. *Biochemical Journal*, *126*(5), 1181–1191. https://doi.org/10.1042/bj1261181

Romanini, D., Kachanov, A. A., Sadeghi, N., & Stoeckel, F. (1997). CW cavity ring down spectroscopy. *Chemical Physics Letters*, *264*(3–4), 316–322. https://doi.org/10.1016/s0009-2614(96)01351-6

Santoro, A. E., Buchwald, C., McIlvin, M. R., & Casciotti, K. L. (2011). Isotopic signature of N_2O produced by marine ammonia-oxidizing archaea. *Science*, *333*(6047), 1282–1285. https://doi.org/10.1126/science.1208239

Sasakawa, M., Tsunogai, U., Kameyama, S., Nakagawa, F., Nojiri, Y., & Tsuda, A. (2008). Carbon isotopic characterization for the origin of excess methane in subsurface seawater. *Journal of Geophysical Research*, *113*, C03012. https://doi.org/10.1029/2007JC004217

Schmale, O., Schneider von Deimling, J., Gülzow, W., Nausch, G., Waniek, J. J., & Rehder, G. (2010). Distribution of methane in the water column of the Baltic Sea. *Geophysical Research Letters*, *37*, L12604. https://doi.org/10.1029/2010GL043115

Schmale, O., Wäge, J., Mohrholz, V., Wasmund, N., Gräwe, U., Rehder, G., et al. (2018). The contribution of zooplankton to methane supersaturation in the oxygenated upper waters of the central Baltic Sea. *Limnology and Oceanography*, *63*(1), 412–430. https://doi.org/10.1002/lno.10640

Schneider, B., Kremling, K., & Duinker, J. C. (1992). CO_2 partial pressure in Northeast Atlantic and adjacent shelf waters: Processes and seasonal variability. *Journal of Marine Systems*, *3*, 453–463. https://doi.org/10.1016/0924-7963(92)90016-2

Scranton, M. I., & Farrington, J. W. (1997). Methane production in the waters off Walvis Bay. *Journal of Geophysical Research*, *82*, 4947–4953. https://doi.org/10.1029/JC082i031p04947

Siegfried, L., Schmidt, M., Mohrholz, V., Pogrzeba, H., Nardini, P., Böttinger, M., & Scheuermann, G. (2019). The tropical-subtropical coupling in the Southeast Atlantic from the perspective of the northern Benguela upwelling system. *PLoS One*, *14*(1), e0210083. https://doi.org/10.1371/journal.pone.0210083

Stawiarski, B., Otto, S., Thiel, V., Gräwe, U., Loick-Wilde, N., Wittenborn, A. K., et al. (2019). Controls on zooplankton methane production in the central Baltic Sea. *Biogeosciences*, *16*(1), 1–16. https://doi.org/10.5194/bg-16-1-2019

Sydeman, W. J., García-Reyes, M., Schoeman, D. S., Rykaczewski, R. R., Thompson, S. A., Black, B. A., & Bograd, S. J. (2014). Climate change and wind intensification in coastal upwelling ecosystems. *Science*, *4*(345), 77–80. https://doi.org/10.1126/science.1251635

Tchipalanga, P., Dengler, M., Brandt, P., Kopte, R., Macuéria, M., Coelho, P., et al. (2018). Eastern boundary circulation and hydrography off Angola—Building Angolan oceanographic capacities. *Bulletin of the American Meteorological Society*, *99*, 1589–1605. https://doi.org/10.1175/BAMS-D-17-0197.1

van der Plas, A. K., Monteiro, P. M. S., & Pascall, A. (2007). Cross shelf biogeochemical characteristics of sediments in the central Benguela and their relationship to overlying water column hypoxia. *African Journal of Marine Science*, *29*, 37–47. https://doi.org/10.2989/ajms.2007.29.1.3.68

Walter, S., Bange, H. W., Breitenbach, U., & Wallace, D. W. R. (2006). Nitrous oxide in the North Atlantic Ocean. *Biogeosciences*, *3*, 607–619. https://doi.org/10.5194/bg-3-607-2006

Walter, S., Bange, H. W., & Wallace, D. W. R. (2004). Nitrous oxide in the surface layer of the tropical North Atlantic Ocean along a west to east transect. *Geophysical Research Letters*, *31*, L23S07. https://doi.org/10.1029/2004GL019937

Wanninkhof, R. (2014). Relationship between wind speed and gas exchange over the ocean revisited. *Limnology and Oceanography: Methods*, *12*(6), 351–362. https://doi.org/10.4319/lom.2014.12.351

Wanninkhof, R., Asher, W. E., Ho, D. T., Sweeney, C. S., & McGillis, W. R. (2009). Advances in quantifying air-sea gas exchange and environmental forcing. *Annual Review of Marine Science*, *1*, 213–244. https://doi.org/10.1146/annurev.marine.010908.163742

Weber, T., Wiseman, N. A., & Kock, A. (2019). Global ocean methane emissions dominated by shallow coastal waters. *Nature Communications*, *10*, 4584. https://doi.org/10.1038/s41467-019-12541-7

Weiss, R. F., & Price, B. A. (1980). Nitrous oxide solubility in water and seawater. *Marine Chemistry*, *8*, 347–359. https://doi.org/10.1016/0304-4203(80)90024-9

Wiesenburg, D. A., & Guinasso, N. L., Jr. (1979). Equilibrium solubilities of methane, carbon monoxide, and hydrogen in water and seawater. *Journal of Chemical and Engineering Data*, *24*, 356–360. https://doi.org/10.1021/je60083a006

Wilson, S. T., Al-Haj, A. N., Bourbonnais, A., Frey, C., Fulweiler, R. W., Kessler, J. D., et al. (2020). Ideas and perspectives: A strategic assessment of methane and nitrous oxide measurements in the marine environment. *Biogeosciences Discussions*, *17*, 1–37. https://doi.org/10.5194/bg-17-5809-2020

Wilson, S. T., Bange, H. W., Arévalo-Martínez, D. L., Barnes, J., Borges, A. V., Brown, I., et al. (2018). An intercomparison of oceanic methane and nitrous oxide measurements. *Biogeosciences*, *15*, 5891–5907. https://doi.org/10.5194/bg-15-5891-2018

Zumft, W. G. (1997). Cell biology and molecular basis of denitrification. *Microbiology and Molecular Biology Reviews*, *61*(4), 533–616. https://doi.org/10.1128/.61.4.533-616.1997